Li et al. Nanoscale Research Letters (2015) 10:111
DOI 10.1186/s11671-015-0821-7

Nanoscale Research Letters
a SpringerOpen Journal

NANO EXPRESS Open Access

Investigation of GaInAs strain reducing layer combined with InAs quantum dots embedded in Ga(In)As subcell of triple junction GaInP/Ga(In)As/Ge solar cell

Senlin Li[1,2,3], Jingfeng Bi[1,2], Mingyang Li[2], Meijia Yang[2], Minghui Song[1,2], Guanzhou Liu[1,2], Weiping Xiong[2], Yang Li[3], Yanyan Fang[3], Changqing Chen[3], Guijiang Lin[1,2*], Wenjun Chen[2], Chaoyu Wu[2] and Duxiang Wang[2]

Abstract

The InAs/GaAs quantum dots structure embedded in GaInP/Ga(In)As/Ge triple junction solar cell with and without $Ga_{0.90}In_{0.10}As$ strain reducing layer was investigated. Conversion efficiency of 33.91% at 1,000 suns AM 1.5D with $Ga_{0.90}In_{0.10}As$ strain reducing layer was demonstrated. A 1.19% improvement of the conversion efficiency was obtained via inserting the $Ga_{0.90}In_{0.10}As$ strain reducing layer. The main contribution of this improvement was from the increase of the short-circuit current, which is caused by the reduction of the Shockley–Read–Hall recombination centers. Consequently, there was a decrease in open circuit voltage due to the lower thermal activation energy of confined carriers in $Ga_{0.9}In_{0.1}As$ than GaAs and a reduction in the effective band gap of quantum dots.

Keywords: InAs quantum dots; Triple junction solar cell; Strain reducing layer; Metal organic chemical vapor deposition

Background

Today's state-of-the-art conversion efficiency of matured lattice-matched GaInP/Ga(In)As/Ge solar cell is 41.6% ± 2.5% at 364 suns concentration and 32.0% ± 1.5% at one sun [1], which have been widely used for terrestrial photovoltaic [2] and space applications [3]. Experimentally, the outdoor module performance had strong relations with the Ga(In)As subcell in CPV power plants. In this case, for further efficiency enhancement, quantum structures such as quantum well [4] and quantum dots (QDs) [5-14] are usually introduced to extend the absorption spectrum to lower energy photons, thus increasing the current density. Additionally, the QDs enhanced devices may improve the radiation tolerance for space application, temperature coefficients, and spectral response under concentration [14-16]. However, the incorporation of quantum structures is usually accompanied by a significant decrease in open-circuit voltage (V_{oc}). For these reasons, numerous efforts have been made inducing a high-potential barriers fence [5-7] and strain compensation technique [9-11]. As reported, the V_{oc} could recover via the decrease in trapping and recombination of carriers in the QDs and wetting layer, which is due to resonant tunneling through a new electronic state created by the fence layer. For the strain compensation technique, the V_{oc} might maintain by the decrease of Shockley-Read-Hall (SRH) recombination that benefit from the less defects. Almost all these mentioned above quantum dots solar cell are based on a GaAs substrate. When InAs/GaAs QD structure is grown on a Ge substrate, GaAs become the natural compensation materials for its lattice constant between InAs and Ge. Nevertheless, the larger lattice mismatch between InAs QDs and GaAs space layer usually induces defects. These defects become the trap center for photon generated carries, thus deteriorating the performance of device. In this paper, a $Ga_{0.90}In_{0.10}As$ strain reducing layer (SRL) was applied to reduce these defects in the QD solar cell. The effects of $Ga_{0.90}In_{0.10}As$ SRL on InAs

* Correspondence: linguijiang@sanan-e.com
[1]Xiamen San'an Optoelectronics Co., Ltd, Xiamen 361009, China
[2]Tianjin San'an Optoelectronics Co., Ltd, Tianjin 300384, China
Full list of author information is available at the end of the article

QDs embedded in GaInP/Ga(In)As/Ge triple junction solar cell (TJSC) were investigated.

Methods

The QD TJSC was fabricated on a 4 in. Ge (001) substrate 9° offcut toward <111> direction via metal organic chemical vapor deposition (MOCVD). As shown in Figure 1, the Ge subcell and *p-i-n* Ga(In)As subcell are connected by the n++GaAs/p++GaAs tunnel junction (TJ), and the *p-i-n* Ga(In)As subcell and GaInP subcell are connected by the n++GaAs/p++AlGaAs TJ. A five-layer InAs QDs with and without $Ga_{0.90}In_{0.10}As$ SRL embedded in the *i*-region of *p-i-n* Ga(In)As subcell was studied.

Prior to the InAs QD structure growth, Ge subcell, n++GaAs/p++GaAs TJ, AlGaAs back surface field, and Ga(In)As base were formed on the Ge substrate, and then a 15 nm intrinsic GaAs was deposited at 620°C. Thereafter, the substrate temperature was lowed 510°C for the InAs QDs growth via Stranski-Krastanov growth mode with a coverage of 1.8 monolayer, followed by a 3 nm $Ga_{0.90}In_{0.10}As$ SRL, an 1 nm CaP strain compensation layer, and an 11 nm GaAs layer, and then the substrate temperature was ramped to 620°C for a high temperature GaAs growth with a thickness of 25 nm. By repeating this sequence, a five periods of InAs QDs were fabricated in the intrinsic region. For the surface and strain analysis, the fifth layer InAs QDs was uncapped, denoted as sample A1. For a comparison, the 3 nm $Ga_{0.90}In_{0.10}As$ SRL in sample A1 was replaced by a 3 nm GaAs layer with all the other growth parameters remained the same, denoted as sample A2. Then, the Ga(In)As emitter and AlGaAs window were deposited, followed by a n++GaAs/p++AlGaAs TJ, GaInP subcell, and GaAs contact layer, completing the QD TJSC growth. The QD TJSC that based on sample A1 is denoted as sample B1, and that based on sample A2 is denoted as sample B2.

Post MOCVD growth, the structure was processed into chips with size of 1×1 cm^2. The front grids were patterned by photolithography and chemical etch with a shadow ratio of 5%, and then the contact metal was deposited by thermal evaporation. Subsequently, an Al_2O_3/Ti_3O_5 dual layer anti-reflection coating (ARC) was evaporated on the front surface of the cells forming the front-side passivation of the top cell to improve the spectral response. All the solar cells were isolated by a chemical etch.

The InAs QD densities and morphologies of sample A1 and A2 were characterized by atomic force microscopy (AFM). The optical performance was measured by a room temperature (RT) photoluminescence (PL). The structural characterization like the strain condition was analyzed by high resolution X-ray diffraction (HRXRD). The external quantum efficiency (EQE) of QD TJSC was measured with a commercial Enlitech system. The current-voltage (I-V) characteristics were measured using a solar simulator at RT under 1,000 suns, low-AOD, AM 1.5D conditions.

Results and discussion

As illustrated in Figure 2, the Ga(In)As and Ge are lattice matched which were confirmed by the single Bragg peak. In both HRXRD spectra, the five period InAs/GaAs QD superlattice (SL) fringe peaks are visible. The zeroth-order peak of sample A1 is buried underneath the Ga(In)As and Ge Bragg peak, but a shift of 140 arcsecond is observed in sample A2, meaning that the five period InAs/GaAs QD SL is under a tensile strain from the substrate. The out-of-plane strain $\varepsilon_{\perp}$ is 1.045‰, which is determined from a differentiated formulation of Bragg's law shown as followed [17]:

$$\varepsilon_{\perp} = \Delta a/a = \Delta\theta_{sl} cot\theta_b \quad (1)$$

Where $\Delta\theta_{sl}$ is the difference in angle between the substrate Bragg peak and the zeroth order SL peak, θ_b is the

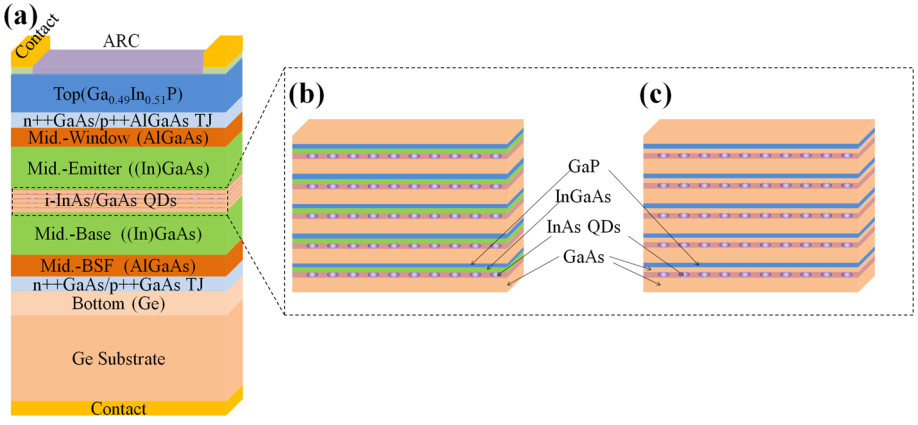

Figure 1 The QD TJSC image. (a) The structure of QD TJSC, QD structure of **(b)** sample A1 with $Ga_{0.90}In_{0.10}As$ SRL, **(c)** sample A2 without $Ga_{0.90}In_{0.10}As$ SRL.

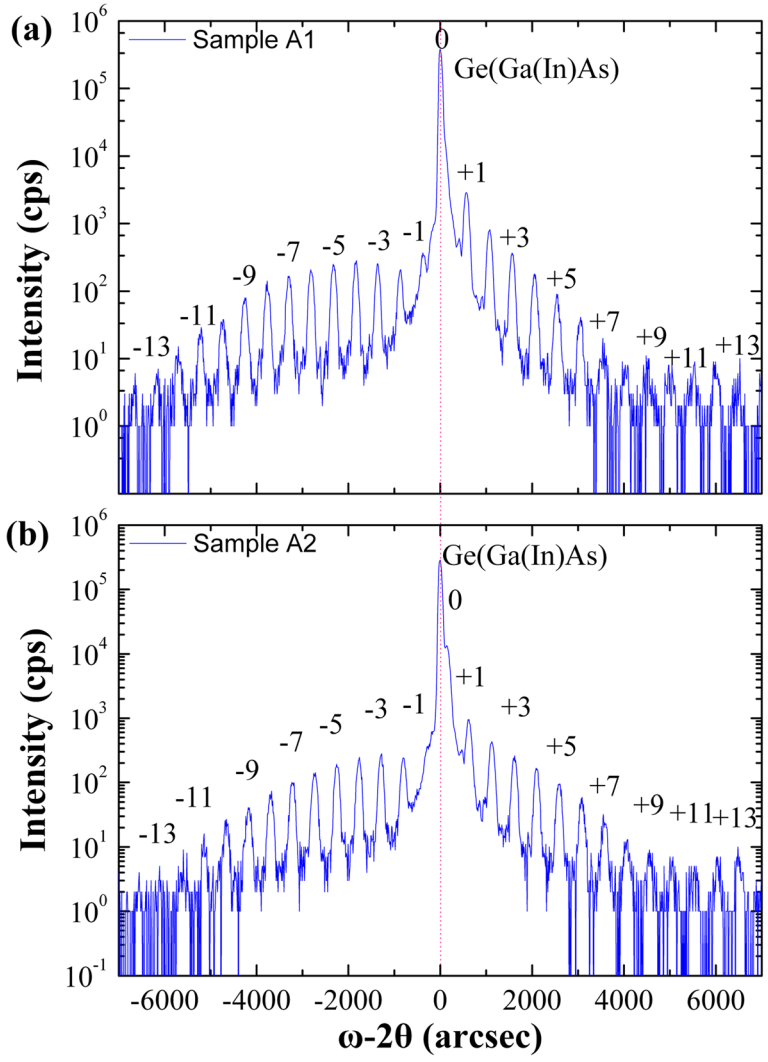

Figure 2 HRXRD of InAs/GaAs QD structure. (a) Sample A1 with $Ga_{0.90}In_{0.10}As$ SRL, **(b)** sample A2 without $Ga_{0.90}In_{0.10}As$ SRL.

value of the substrate Bragg angle, and Δa/a is the fractional lattice mismatch representing the out-of-plane strain of the SL. Corresponding the in-plane strain $\varepsilon_{//}$ (1.136‰) of InAs QDs can be estimated by the equation [18]

$$\varepsilon_{\perp} = -2\frac{C_{12}}{C_{11}}\varepsilon_{//} \tag{2}$$

These results suggested that more defects may be formed in the QD TJSC without $Ga_{0.90}In_{0.10}As$ SRL.

Figures 3a and b show the 2 × 2 μm AFM images of QDs with and without $Ga_{0.90}In_{0.10}As$ SRL. The corresponding room temperature PL spectra are plotted in Figure 4. By inserting an $Ga_{0.90}In_{0.10}As$ SRL, the InAs QD density of sample A1 is increased from 8.1×10^9 cm^{-2} (sample A2) to 1.2×10^{10} cm^{-2} (sample A1), which is consistent with the PL intensity. As is well known, the strain fields created by the QDs in the first layer strongly influence the QD nucleation on the second layer [19]. The increasing of the QD density of sample A1 with $Ga_{0.90}In_{0.10}As$ SRL can be ascribed to the reduction of the accumulated strain field, which is assumed by the strain as interpreted by the XRD results. Correspondingly, the PL intensity of QDs is improved by the inserting of $Ga_{0.90}In_{0.10}As$ SRL. For one reason, the QD density is increased. Secondly, less defects may be existed in sample A1 due to the decrease of lattice mismatch, leading to less SRH recombination centers [20]. These two reasons induced a better optical performance of sample A1. In addition, the PL peak of sample A1 exhibits a red shift of about 3 meV with respect to samples A2. The following reasons may need to be considered: Firstly, the relief of the compressive strain conducted a 1.94 meV red shift to the band energy, which is calculated by the following equation [21],

$$\Delta E_0 = 1.71\varepsilon(eV) \tag{3}$$

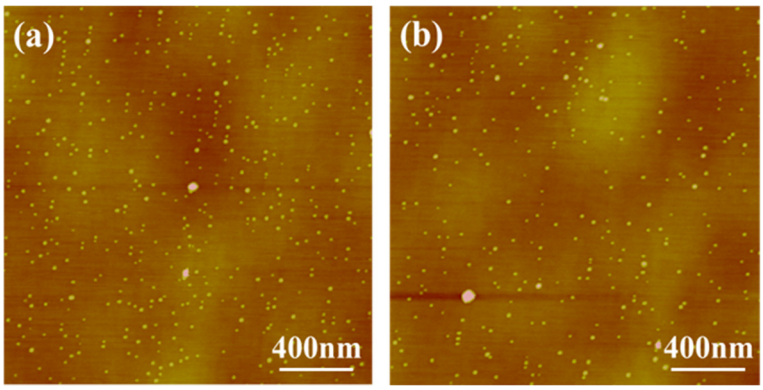

Figure 3 The 2 × 2 μm AFM images of the fifth layer InAs QDs. (a) Sample A1 with $Ga_{0.90}In_{0.10}As$ SRL, **(b)** sample A2 without $Ga_{0.90}In_{0.10}As$ SRL.

Secondly, the $Ga_{0.90}In_{0.10}As$ SRL could suppress the In/Ga inter-diffusion [22] compared to GaAs, thus conducting a less blue-shift. At last, the less quantum confinement of GaInAs [23] than GaAs will result in a red shift to the QDs.

As shown in Figure 5, the top cell in the QD TJSC with and without a $Ga_{0.90}In_{0.10}As$ SRL yields EQE of 12.65 and 12.55 mA/cm^2, respectively. The relative lower EQE of the top cell without $Ga_{0.90}In_{0.10}As$ s SRL may be caused by the deteriorated crystalline quality of GaInP [24], which was affected by the strained InAs/GaAs QD SL in the middle cell. The EQE of the middle cell is 11.16 and 10.51 mA/cm^2 in sample B1 and sample B2, respectively, and exhibits absorption edge at 950 nm. This extended absorption range is due to the QDs absorption, whose threshold wavelength is in agreement with the QD ground state transition. The spectral response of the wetting layer and QD ground state transitions is approximately 5% and approximately 1%, respectively. Remarkably, the middle cell with $Ga_{0.90}In_{0.10}As$ SRL yields higher EQE response (about 75%) than that without $Ga_{0.90}In_{0.10}As$ SRL (about 70%) in the spectral region below 880 nm, which can be attributed to the less defects in sample B1 and thus reduced the SRH recombination of photon generated carriers. The EQE of the bottom cell in the QD TJSC with and without $Ga_{0.90}In_{0.10}As$ SRL shows an equal value at 17.2 mA/cm^2 and a spectral response of approximately 73%. In comparison with top cell, the Ge bottom cell has a relative lower spectral response. Because the Ge bottom cell is indirect band gap semiconductor that has a short minority carrier diffusion lengths and short minority carrier lifetimes [25]. In a word, the short-circuit current (I_{sc}) of the QD TJSC in this case is limited by the middle cell, suggesting that the effects of $Ga_{0.90}In_{0.10}As$ SRL on current of the middle cell is significant to the final I_{sc} of the QD TJSC.

Figure 6a shows the I-V characteristics of the QD TJSC under 1,000 suns. The values of open-circuit voltage (V_{oc}), fill factor (FF), short-circuit current (I_{sc}), and convention efficiency (η) are listed in Table 1. The I_{sc} of sample B1 is 12.79 A, and a 2.73% higher than that of sample B2. As mentioned above, the crystalline quality is improved by inserting of a $Ga_{0.90}In_{0.10}As$ SRL with reduced the defects. So the improvement of I_{sc} is assumed

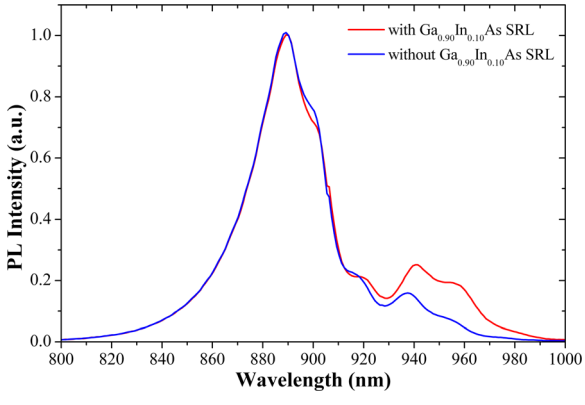

Figure 4 PL spectra of InAs/GaAs QDs with and without $Ga_{0.90}In_{0.10}As$ SRL.

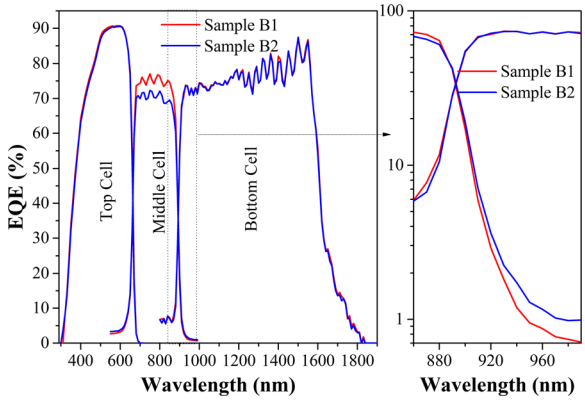

Figure 5 EQE of QD TJSC with and without $Ga_{0.90}In_{0.10}As$ SRL.

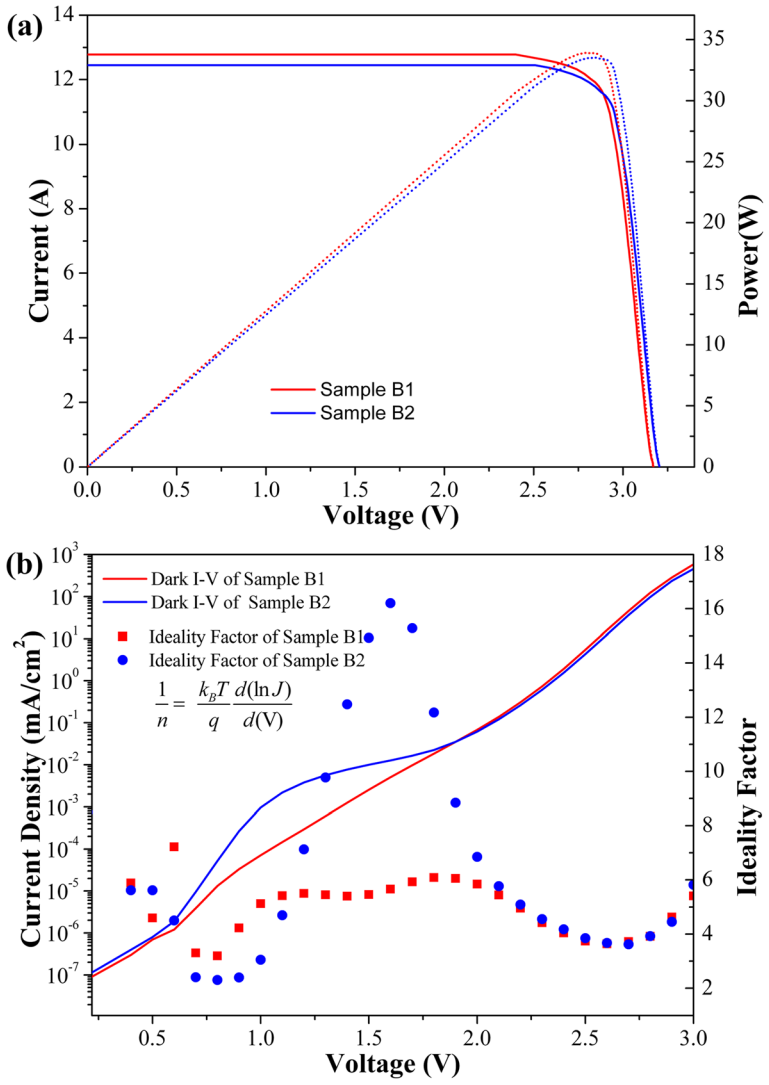

Figure 6 The I-V measurements and dark I-V curves. (a) I-V measurements at 1,000 suns AM 1.5D of QD TJSC with and without $Ga_{0.90}In_{0.10}As$ SRL, **(b)** dark I-V curves and the corresponding ideality factor of QD TJSC with and without $Ga_{0.90}In_{0.10}As$ SRL.

due to the reduction in SRH recombination that originated from the defects, which is in well agreement with the EQE characterization as shown in Figure 5. To further clarify this speculation, the dark I-V was measured by Keithley system and displayed in Figure 6b. As we can see that the two I-V curves are almost overlapped with each other. The only difference is the hump that appears at the sample B2 with respecting the different epitaxial structure of $Ga_{0.90}In_{0.10}As$ SRL layer. Know to all, the corresponding ideality factor (n) as a function of applied voltage is described as Equation 4:

$$\frac{1}{n} = \frac{k_B T}{q} \frac{d(lnJ)}{d(V)} \tag{4}$$

Where the k_B is the Boltzmann constant, q is the elementary charge, and J is the current density. As illustrated in Figure 6b, the ideality factor of the sample without $Ga_{0.90}In_{0.10}As$ SRL is varied from 2 to 16 at a low forward voltage bias (1.2~1.9 V hump area), but the one from sample B1 almost remains constant. The large ideality factor ($n > 10$) in the sample without $Ga_{0.90}In_{0.10}As$ SRL suggests that more SRH recombination is occurred [26]. Notably, the V_{oc} of sample B1 is 30 mV lower than that of sample B2. The difference in V_{oc} between samples with (B1) and without (B2) $Ga_{0.90}In_{0.10}As$ SRL is larger

Table 1 The open-circuit voltage (V_{oc}), fill factor (FF), short-circuit current (I_{sc}), and conversion efficiency (η) of QD TJSC

No.	I_{sc}(A)	V_{oc}(V)	FF(%)	η(%)
Sample B1	12.79	3.17	83.69	33.91
Sample B2	12.45	3.20	84.01	33.51

than that in InAs ground state energy observed in PL. So the fact that the $In_{0.1}Ga_{0.9}As$ SRL has lower band energy relative to GaAs and consequently decreases the thermal activation energy of confined carriers need to be considered in the case. Nevertheless, by inserting $Ga_{0.90}In_{0.10}As$ SRL, conversion efficiency of GaInP/Ga(In)As/Ge TJSC embedded with InAs QDs is improved by 1.19% relatively and arrive at 33.91% under 1,000 suns AM 1.5D.

Conclusions

In summary, the InAs/GaAs QDs structures embedded in GaInP/Ga(In)As/Ge TJSC with and without $Ga_{0.90}In_{0.10}As$ SRL were investigated. The QD density was increased and a red shift of the QD illumination peak was observed by inserting a $Ga_{0.90}In_{0.10}As$ SRL. Also, the strain was reduced by the inserting of $Ga_{0.90}In_{0.10}As$ SRL. Although a reduction in V_{oc} was observed in the sample B1 due to the decrease of thermal activation energy of confined carriers of $Ga_{0.90}In_{0.10}As$ SRL and a reduction in the total energy band gap, the conversion efficiency of QD TJSC is improved by 1.19% relatively via inserting the $Ga_{0.90}In_{0.10}As$ SRL. The cell with $Ga_{0.90}In_{0.10}As$ SRL showed an improved device quality and reduced SRH recombination of photon generated carriers, thus resulted in a large increase of I_{sc}. Finally, the QD TJSC with $Ga_{0.90}In_{0.10}As$ SRL has demonstrated a conversion efficiency of 33.91% at 1,000 suns AM 1.5D.

Abbreviations

AFM: atomic force microscope; ARC: anti-reflection coating; I-V: current-voltage; EQE: external quantum efficiency; η: efficiency; FF: fill factor; HRXRD: high resolution x-ray diffraction; MOCVD: metal organic chemical vapor deposition; QDs: quantum dots; RT: room temperature; I_{sc}: short-circuit current; SRH: Shockley-Read-Hall; SRL: strain reducing layer; SL: super lattice; TJ: tunnel junction; TJSC: triple junction solar cell; V_{oc}: open-circuit voltage.

Competing interests

The authors declare that they have no competing interests.

Authors' contributions

LSL wrote the manuscript and participated in the growth of solar cell and the data analysis. BJF and SMH participated in the results discussions and sample preparation. LMY, YMJ, LGZ, and XWP took part in the discussions and the chip process. LY participated in the dark I-V test. BJF, FYY, CCQ, LGJ, CWJ, WCY, and WDX supervised the writing of the manuscript and all the experiments. All authors read and approved the final manuscript.

Acknowledgements

This work was supported by a grand from the National High Technology Research and Development Program of China (863 programs) (No. 2012AA051402).

Author details

[1]Xiamen San'an Optoelectronics Co., Ltd, Xiamen 361009, China. [2]Tianjin San'an Optoelectronics Co., Ltd, Tianjin 300384, China. [3]Wuhan National Laboratory for Optoelectronics, School of Optical and Electronic Information, Huazhong University of Science and Technology, Wuhan 430074, China.

Received: 12 January 2015 Accepted: 14 February 2015
Published online: 07 March 2015

References

1. Green MA, Emery K, Hishikawa Y, Warta W. Solar cell efficiency tables (version 37). Prog Photovolt Res Appl. 2011;19:84–92.
2. Bosi M, Pelosi C. The potential of III-V semiconductors as terrestrial photovoltaic devices. Prog Photovolt Res Appl. 2007;15:51–68.
3. Takamoto T, Kaneiwa M, Imaizumi M, Yamaguchi M. InGaP/GaAs-based multijunction solar cells. Prog Photovolt Res Appl. 2005;13:495–511.
4. Fujii H, Toprasertpong K, Wang Y, Watanabe K, Sugiyama M, Nakano Y. 00-period, 1.23-eV bandgap InGaAs/GaAsP quantum wells for high-efficiency GaAs solar cells: toward current-matched Ge-based tandem cells. Prog Photovolt Res Appl. 2014;22:784–95.
5. Wei G, Forrest SR. Intermediate-band solar cells employing quantum dots embedded in an energy fence barrier. Nano Lett. 2007;7:218–22.
6. Sablon KA, Little JW, Olver KA, Wang ZM, Dorogan VG, Mazur YI, et al. Effects of AlGaAs energy barriers on InAs/GaAs quantum dot solar cells. J Appl Phys. 2010;108:074305.
7. Tutu FK, Lam P, Wu J, Miyashita N, Okada Y, Lee K-H, et al. InAs/GaAs quantum dot solar cell with an AlAs cap layer. Appl Phys Lett. 2013;102:163907.
8. Linares PG, Martí A, Antolín E, Farmer CD, Ramiro Í, Stanley CR, et al. Voltage recovery in intermediate band solar cells. Sol Energ Mat Sol C. 2012;98:240–4.
9. Hubbard SM, Cress CD, Bailey CG, Raffaelle RP, Bailey SG, Wilt DM. Effect of strain compensation on quantum dot enhanced GaAs solar cells. Appl Phys Lett. 2008;92:123512.
10. Laghumavarapu RB, El-Emawy M, Nuntawong N, Moscho A, Lester LF, Huffaker DL. Improved device performance of InAs/GaAs quantum dot solar cells with GaP strain compensation layers. Appl Phys Lett. 2007;91:243115.
11. Oshima R, Takata A, Okada Y. Strain-compensated InAs/GaNAs quantum dots for use in high-efficiency solar cells. Appl Phys Lett. 2008;93:083111.
12. Bailey CG, Forbes DV, Raffaelle RP, Hubbard SM. Near 1 V open circuit voltage InAs/GaAs quantum dot solar cells. Appl Phys Lett. 2011;98:163105.
13. Tanabe K, Guimard D, Bordel D, Arakawa Y. High-efficiency InAs/GaAs quantum dot solar cells by metalorganic chemical vapor deposition. Appl Phys Lett. 2012;100:193905.
14. Hubbard SM, Bailey CG, Aguinaldo R, Polly S, Forbes DV, Raffaelle RP. Characterization of quantum dot enhanced solar cells for concentrator photovoltaics. In: Photovoltaic Specialists Conference (PVSC), 2009 34th IEEE. 2009. p. 000090–5.
15. Cress CD, Hubbard SM, Landi BJ, Raffaelle RP, Wilt DM. Quantum dot solar cell tolerance to alpha-particle irradiation. Appl Phys Lett. 2007;91:183108.
16. Sogabe T, Shoji Y, Ohba M, Yoshida K, Tamaki R, Hong HF, et al. Intermediate-band dynamics of quantum dots solar cell in concentrator photovoltaic modules. Sci Rep. 2014;4:4792.
17. Bailey CG, Hubbard SM, Forbes DV, Raffaelle RP. Evaluation of strain balancing layer thickness for InAs/GaAs quantum dot arrays using high resolution x-ray diffraction and photoluminescence. Appl Phys Lett. 2009;95:203110.
18. Ekins-Daukes NJ, Kawaguchi K, Zhang J. Strain-balanced criteria for multiple quantum well structures and its signature in X-ray rocking curves. Cryst Growth Des. 2002;2:287–92.
19. Howe P. Competition between strain-induced and temperature-controlled nucleation of InAs/GaAs quantum dots. J Appl Phys. 2004;95:2998.
20. Ng JT, Bangert U, Missous M. Formation and role of defects in stacked large binary InAs/GaAs quantum dot structures. Semicond Sci Tech. 2007;22:80–5.
21. Torchynska TV. Photoluminescence peculiarities in InGaAs/GaAs structures with different InAs quantum dot densities. J Lumin. 2013;136:75–9.
22. Litvinov D, Blank H, Schneider R, Gerthsen D, Vallaitis T, Leuthold J, et al. Influence of InGaAs cap layers with different In concentration on the properties of InGaAs quantum dots. J Appl Phys. 2008;103:083532.
23. Yin Z, Tang X, Liu W, Zhang D, Du A. Effects of $In_xGa_{1-x}As$ matrix layer on InAs quantum dot formation and their emission wavelength. J Appl Phys. 2006;100:033109.
24. Kerestes C, Polly S, Forbes D, Bailey C, Podell A, Spann J, et al. Fabrication and analysis multijunction solar cell with an InGaAs Quantum dots junction. Prog Photovolt Res Appl. 2014;22:1172–9.
25. Dimroth F, Kurtz S. High-efficiency multijunction solar cells. MRS Bull. 2007;32:230–5.
26. Kim H, Park MH, Park SJ, Kim HS, Song JD, Kim SH, et al. Influence of InAs quantum dots on the transport properties of GaAs-based solar cell devices. Curr Appl Phys. 2014;14:192–5.